https://doi.org/10.33472/AFJBS.6.6.2024.118-133

African Journal of Biological Sciences

Evaluation of the Trends Variance of Atmospheric Environment using 'MAKESENS' Model with Spatiotemporal Seasonal Analysis over Iraq 2003-2021

Maha S. Hachim[1*], Jasim M. Rajab[1], Ali M. Al-Salihi[1]

[1]Department of Atmospheric Sciences, College of Science, Mustansiriyah University, Baghdad, Iraq. E-mail: Maha.alsultan8@gmail.com

Article History
Volume 6,Issue 6, Feb 2024
Received:01 Mar 2024
Accepted : 08 Mar 2024
doi:10.33472/AFJBS.6.6.2024.118-133

Abstract

The study investigated the seasonal patterns and trends of Tropospheric Ozone (O3) in Iraq between 2003 and 2021, using monthly concentration data from three selected stations. The analysis included other parameters such as Skin Temperature (Skin Temp.), Carbon Monoxide (CO), and Water Vapor (H2O vapor), to assess the impact of weather factors, seasonal patterns, and trends of these parameters. The study unveiled significant changes in the values of these parameters over time across the research area during the 19-year period, with high values occurring in summer and low values in winter for Skin Temperature and Water Vapor. The maximum values of O3 were observed in spring, while the minimum values were in winter. On the other hand, CO exhibited the highest values in winter and the lowest values in fall. The spatial average values of all parameters, except for Skin Temperature, were higher in the northern regions and lower in the southern regions of Iraq. Additionally, trend analysis revealed an increasing trend in Skin Temperature and Water Vapor. The general trend of O3 appeared to be almost constant, with no statistically significant trend. Finally, the CO trend analyses for all stations exhibited a significant negative trend, indicating a decrease in CO concentration over time. These findings provide valuable insights into the seasonal patterns and trends of Tropospheric parameters air quality in Iraq and can inform policymakers in developing effective air quality management strategies.

Keywords: *Atmospheric environment, MAKESENS, AIRS, Iraq.*

1. Introduction

The passage discusses the crucial role of ozone in shielding life on Earth from harmful ultraviolet radiation from the sun. It distinguishes between two types of ozone: tropospheric ozone and stratospheric ozone. Tropospheric ozone is primarily found in the lower atmosphere, formed through chemical reactions involving human and natural origins of pollutants including oils, organic compounds such as (VOCs), and nitrogen oxides (NOx). It is a pollutant that is associated with detrimental effects on personal health, vegetation, and ecosystems, causing ventilator problems and contributing to the formation of smog, as well as Absorbing infrared

radiation that contributes to global warming. On the other hand, the stratospheric ozone layer, naturally formed through the process by which UV radiation from the sun reacts with oxygen in the upper atmosphere (stratosphere), acts as a protective shield for the Earth, protecting against negative effects of UV exposure from reaching the Earth's surface. However, human-made chemicals like chlorofluorocarbons (CFCs) have caused a significant depletion of stratospheric ozone, leading to increased levels of harmful UV radiation that makes it through the Earth's atmosphere, causing health problems such as skin cancer and cataracts. Therefore, while both tropospheric and stratospheric ozone are crucial elements of the Earth's atmosphere, they have significant differences in their formation, function, and impact on human health and the environment (Stock et al. 2013, Rajab, Lim and MatJafri 2013, Safieddine et al. 2016, Vollmer et al. 2021, Kirschke et al. 2013, Fiore et al. 2012, Liu et al. 2022, Strahan and Douglass 2018). The factors affecting the concentration and distribution of tropospheric ozone, such as temperature, sunlight, wind, humidity, and pollutants like NO_x and VOCs emitted from human activities and natural sources (Rajab et al. 2011c, Rajab et al. 2020, Borhani et al. 2021, Chen et al. 2023). Global warming should result in the rise of average land surface temperatures worldwide and surface-atmosphere interactions play a crucial role in determining and influencing two types of surface temperatures: surface air temperature (Tair) and skin temperature (Tskin). Climatological data can be developed for both these temperature measures. The term "skin temperature," which is synonymous with "radiometric surface temperature," can be assessed through various means. It is obtainable using a handheld or aircraft-mounted radiation thermometer, derived from upward long-wave radiation and governed by the Stefan-Boltzmann law. Additionally, satellite observations can be utilized to map skin temperature over extensive regions after compensating for atmospheric attenuation effects on the measured radiances. Over the past two decades, the techniques used to retrieve Tskin (skin temperature) from satellite measurements for land applications have undergone significant advancements. Many Tskin algorithms now offer improved accuracy, with deviations of only 0.5 to 1°C for field measurements and satellite observations conducted under clear sky conditions (Jin and Dickinson 2002, Jin, Dickinson and Zhang 2005, Lim et al.,2008, Jin and Dickinson 2010, Gulev et al. 2021, Ali et al., 2021, Lim et al., 2022, Panos et al., 2023). Apart from the six greenhouse gases covered by the Kyoto Protocol, climate change is also influenced significantly by tropospheric O_3 precursors such as CO, NMVOC, CO2, and NO_x, as well as black carbon, organic carbon, and SO_2. A positive correlation has been observed between ozone and CO (Rypdal et al. 2005, Kajii et al. 1998, Rajab et al. 2011a, Rajab et al. 2011b, Salih, Al-Salihi and Rajab 2018, Al-Bayati and Al-Salihi 2019, Abdulfattah et al. 2020, Lim et al., 2022, Abbas and Rajab 2022). The study on the impact of temperature and water vapor on surface O_3 and NO_x demonstrates a direct association with temperature, which acts as an indicator of the intensity of incident solar radiation and, consequently, the effectiveness of photochemical processes.

The research reveals a positive correlation between O_3 and temperature, with a coefficient of approximately 0.77. The strong connection between ozone concentration and temperature has been thoroughly established and is supported by solid theoretical foundations. Abundant experimental evidence further confirms the positive correlation between ozone and temperature. Additionally, the presence of water vapor in the atmosphere plays a vital role in both the formation and depletion of ozone (David and Nair 2011, Al-Salihi, Rajab and Salih 2019). Satellite remote sensing is an increasingly popular method employed by environmental scientists to monitor environmental changes continuously. This technique utilizes Earth-orbiting satellites to swiftly and regularly collect data, offering a comprehensive global view of environmental

concerns and delivering high-resolution data across various wavelengths of the electromagnetic spectrum. Utilizing this technology, scientists can make estimations of atmospheric gas concentrations, monitor their spatial and temporal fluctuations, pinpoint their origins and sinks, and observe alterations within the Earth's climate system. (Lu et al. 2021, Stavert et al. 2022).

2. Materials and methods

Iraq shares boundaries with Turkey and Iran to the north and east, respectively, and is adjacent to Kuwait, Saudi Arabia, Jordan, and Syria to the southeast, south, west, and northwest, respectively. Baghdad is the capital. The weather is predominantly dry and semi-dry, with sweltering summers and mild winters. Certain regions in the north experience different climatic conditions receive winter snowfall, while summer temperatures can exceed 50°C (122°F) in some parts of the country (Abbas, Wasimia and Al-Ansari 2016, Azooz, Talal and Development 2015, Salman et al. 2022, Firas 2022). During summer in Iraq, particularly in the southern and eastern regions, temperatures can exceed 50°C (122°F). Winter temperatures are milder, with occasional snowfall in some northern regions. Annual precipitation is generally low, with most areas receiving less than 250 mm (10 inches), although some northern mountainous regions can receive up to 600 mm (24 inches) of rainfall annually. Dust and sandstorms can occur during summer, and the Tigris and Euphrates rivers are prone to winter flooding. Iraq's climate is generally hot and dry in summer, mild in winter, and characterized by low precipitation levels, with regional variations in temperature and rainfall, as well as occasional dust and sandstorms and flooding in certain areas (Al-Faraj, Tigkas and Scholz 2016, Al Khudhairy 2018, Abdulfattah et al. 2020, Kadhum et al. 2022). The O_3, Skin Temp., CO and H_2O vapor data were collected for Iraq from the AIRS3STM_006_ files with a spatial resolution of 1^o x 1^o, covering the period of 2003-2021. The Monthly data for three main cities in Iraq, Including Mosul, Baghdad, and Basra were utilized. AIRS is a highly sensitive instrument on NASA's Aqua satellite that measures various atmospheric parameters using its 2378 spectral channels, providing accurate measurements of temperature, humidity, and trace gases like O_3, CO, and CH_4. Its data have been used extensively by scientists worldwide to study atmospheric phenomena, including climate change, weather patterns, and air pollution (Aumann et al. 2003, Rajab et al., 2011a, Susskind et al. 2019). The Finnish Meteorological Institute developed MAKESENS 1.0 identifying and estimating patterns in time series data atmospheric chemical component concentrations. The software employs non-parametric statistical techniques, such as the Mann-Kendall test and Sen's non-parametric method, to examine monotonic patterns and calculate linear trend slopes. These methods offer several advantages, such as their ability to handle missing values and not necessitating data to follow a specific distribution.

Additionally, Sen's method is less influenced by outliers and isolated data errors, enhancing its robustness in data analysis (Gilbert 1987, Park et al., 2011, Rahman et al., 2016, and Mojid et al., 2019). The test statistic Z can be expressed as follows:

$$\left.\begin{array}{ll} Z = S - \frac{1}{\sqrt{VAR(S)}} & \text{If} \quad S > 0 \\ Z = 0 & \text{If} \quad S = 0 \\ Z = S + 1/\sqrt{VAR(S)} & \text{If} \quad S > 0 \end{array}\right\} \quad \ldots\ldots\ldots (1)$$

The Z value is utilized to ascertain the presence of a statistically significant trend, where a positive (negative) value indicates a pattern of increase (decrease). At the α significance level, a

two-sided test is conducted, and the null hypothesis is rejected when the absolute value of Z exceeds Z1-α/2 obtained from the standard normal distribution tables. The Sen's nonparametric method is employed to determine the reliable slope of an existing straight-line pattern, capturing the yearly variations (Salmi 2002). This indicates that the function f(t) in the following equation holds the same meaning as:

$$f(t)=B+ Qt \ldots\ldots. \quad (2)$$

Where B is a constant, and Q represents the slope. To compute the gradient estimate, denoted as Q above, start by evaluating the slope from the equation:

$$Q = xj-xk/j-k \ldots\ldots. (3)$$

If we assume that j > k and there are n values of xj in the time series, we can obtain N = n(n-1)/2 slope estimates of Qi. The Sen's gradient estimate is calculated as the average of these N Qi values, which are sorted from smallest to largest. The Sen's estimator is then represented as follows:

$$Q=Q[(N+1)/2] \text{ , if N is odd} \ldots\ldots\ldots (4) \qquad \text{Or}$$

$$Q=1/2[(N/2)+Q((N+2)/2)] \ldots\ldots\ldots (5) \qquad \text{If N is even}$$

In MAKESENS, two separate confidence intervals are computed using α values of 0.01 and 0.05, leading to distinct intervals. To estimate B in equation (2), n values of the differences xi - Qti are calculated. The average of these values provides an estimation of B. Similarly, the confidence intervals for B are computed in a comparable manner, resulting in estimates falling within the range of 95% to 99% confidence intervals. (Salmi 2002).

3. Results

Monthly Variation: Figure 1 displays the surface mixing ratio of mean monthly O_3, Skin Temp, CO and H_2O vapor. For the entire study area and 19-year period, the annual means of tropospheric O_3, Skin Temp, CO and H_2O-vapor surface mixing ratio are presented in Table 1.

The mean values for monthly O_3, Skin Temp, CO and H_2O-vapor surface mixing ratio in the study area were (0.04 ± 0.002) ppmv, (310.85 ± 5.11) k, (0.123 ± 0.005) ppmv, and (4.99 ± 0.47) g/kg, respectively. As depicted in Figure 1.a, the O3 values exhibit a seasonal pattern, with higher measurements during the spring and summer months and lower measurements during the fall and winter months for the three cities under consideration. The peak O3 values were recorded in April and May in Mosul (0.051 ppmv), while the minimum values were observed in December in both Mosul and Baghdad (0.032 ppmv). The periodic fluctuations are mainly influenced by meteorological elements, chemistry, and ozone precursors. The data indicates that the city Mosul experienced the highest O_3 levels, followed by Baghdad. Basra registered the lowest O_3 levels, primarily due to the presence of an O_3 sink caused by factors such as Chlorofluorocarbons (CFCs) leading to surface deposition. Additionally, the city's lower O_3 levels can be attributed to the increased emission of gaseous pollutants from petroleum refineries located in the area. Figure 1b shows elevated Skin Temperature readings during summer and fall and lower readings during winter across most stations. The highest values were recorded between June and August in Basra and Baghdad (329.72 W/m^2), while the lowest values were noted in January in Mosul (287.91W/m_2). Figure 1c illustrates significant seasonal variations in CO values, with the highest values in February and March in Mosul (0.151 ppmv) and the minimum number in October in Basra (0.095 ppmv). Figure 1d illustrates the seasonal variations in H_2O vapor levels, with peak readings occurring during the summer months (July-August) and the lowest readings observed during the winter period (December-February) at each location.

Table 1. The annual means of tropospheric O_3, Skin Temp, CO and H_2O vapor surface mixing ratio of Iraq stations for the study period, along with their corresponding standard.

Stations	Long. (E◦)	Lat. (N◦)	Altitude (m)	O_3 (ppmv)		Skin Temp. (k)		CO (ppmv)		H_2O vapor (g/kg)	
				Mean	SD	Mean	SD	Mean	SD	Mean	SD
Mosul	43.06	36.21	223	0.043	0.003	308	14	0.126	0.02	4.783	0.87
Baghdad	44.40	33.30	32	0.042	0.005	311	12	0.119	0.02	4.899	0.81
Basra	47.78	30.30	2	0.041	0.004	314	12	0.116	0.01	4.847	0.57

The highest recorded H_2O-vapor value of 6.44 g/kg was observed during July and August in Baghdad, while the lowest readings of 3.43 mg/kg occurred in January and December in Mosul. Basra exhibited its lowest H_2O-vapor values between May and October. Time Series of Temporal Distribution: The estimated trends and the monthly time series for mean ozone, skin temperature, CO and H_2Ovapor mixing ratio are shown in (Figure 2).and Table 2,3,4,5 All parameter values, except CO, The data demonstrates a monthly variation, reaching its peak during the summer months (July-August) and hitting its lowest point during the winter (December-February) across all the stations under examination. This pattern can be effectively explained by the periodic changes in weather conditions and the local topography. The trend analyses for O_3 across all the stations (Figure 2a) reveal seasonal variations, with the highest values (0.054 ppmv) observed during the spring season and the lowest values (0.032 ppmv) recorded during the winter season. the winter minimum of O_3 can be interpreted as a direct effect of the O_3 sink by surface deposition where suitable conditions for photochemical loss (low temperature, low humidity, and low solar radiation) exist. The overall general trend seems be almost constant where no statistically significant trend is seen (Table 2). Generally, as shown in Figure 2.a there is a zonal variability represented by the highest values of O_3 over regions of higher latitude as Mosul and tendency to decrease downward to the low latitude (Baghdad and Basra)

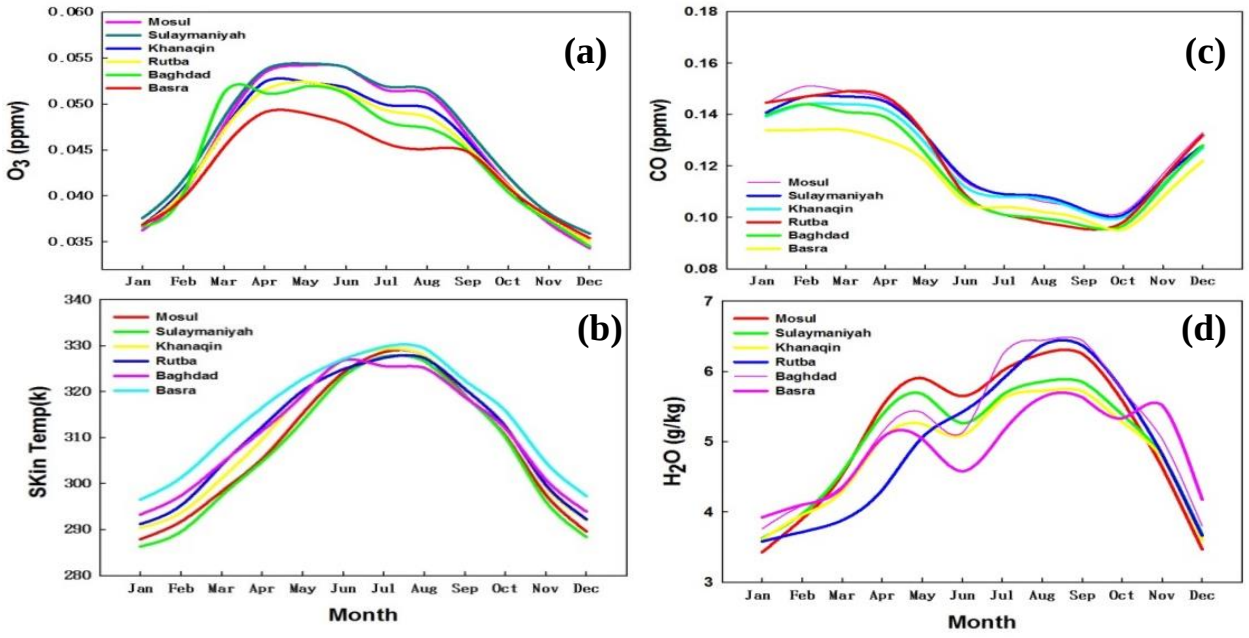

Figure 1. Tropospheric mixing ratios of (a) ozone, (b) skin temperature, (c) CO, (d) H2O-vapor at selected Iraq stations.

The Skin Temperature trend analyses for all considered stations (Figure 2, b) Experiencing notable interannual variability, the values demonstrate a minimum during winter and a maximum during June and July. The annual trend is almost stable during 2003 until 2021 while however, higher values occur in station Basra (329 K). the minimum in Mosul station (286) K reveals increasing trend in Skin Temperature over most of the stations, the increasing trend per year as tabulated in (table 3) ranged from (0.14 – 3.85) K. The CO trend analyses for all the stations exhibit substantial interannual variability, with the minimum values occurring during May to October and the maximum values during February to April. The annual trend analysis observed a stagnation and stability feature as obvious in Figure 2.c) From 2003 until 2007, surface CO levels exhibited a declining trend, which continued to decrease from 2008 until 2021.

These declining trends in surface CO across Iraq during the study period align with the global CO trend reported by the NOAA (National Oceanic and Atmospheric Administration) network. The CO trend analyses for all stations were estimated and indicated a significant negative trend ranging from -2.54 to -5.18 ppmv per year, as shown in Table 4. Figure 2.d: The H_2Ovapor showed fluctuations between months over the study area. Maximum values occur in 2005, 2006, 2015, 2018, 2019 and 2020 in the northern regions (Mosul) in 2010, 2014, 2018 and 2020 while 2006, 2009, 2014, 2018, 2019 and 2020 in Baghdad, finely in Basra at 2008, 2015, 2018 and 2019. The minimum values in 2011 for Baghdad and Basra, and 2009, 2017 in Mosul. These varieties in H_2Ovapor were driven primarily by the changes in meteorology conditions. A more careful examination reveals subtle differences in the H_2Ovapor spatial patterns for each of the peak years; higher values for H_2Ovapor were observed in the summer season than in the winter season. As higher summer temperature results in increased capacity of the atmosphere to hold more water vapor. The trend analyses for H_2O vapor across all stations were calculated, revealing a positive trend ranging from 0.49 to 3.15 g/kg per year, as shown in Table 5.

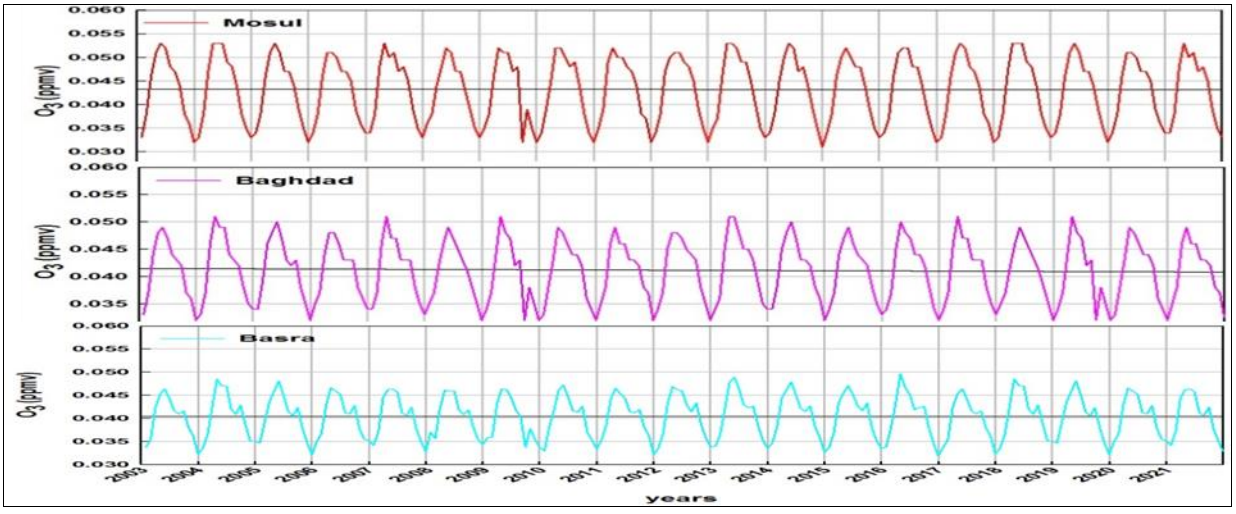

Figure 2.a. Time Series Analysis Ozone concentration over Iraq (2003 -2021).

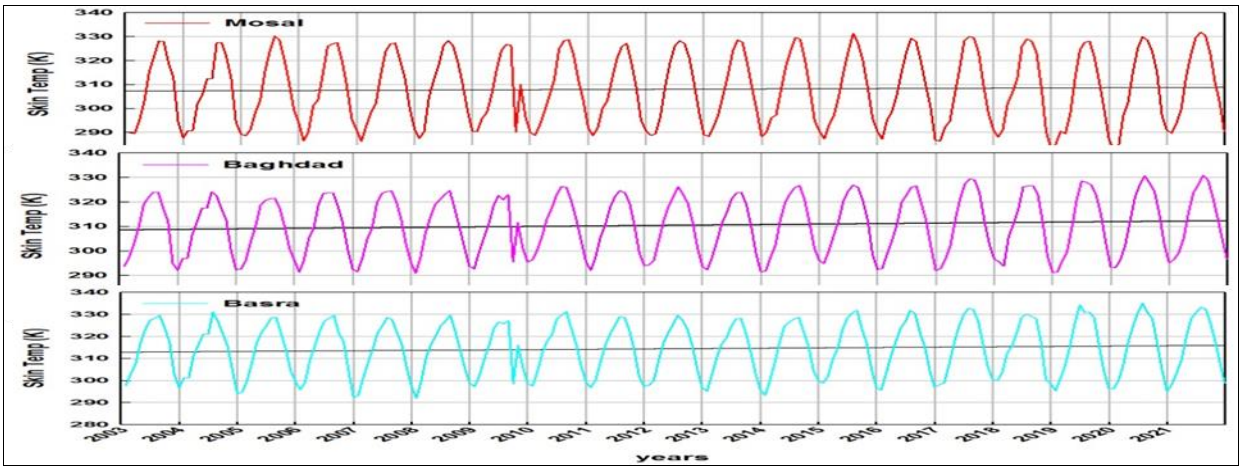

Figure 2.b. Time Series Analysis Skin Temperature concentration over Iraq (2003 -2021).

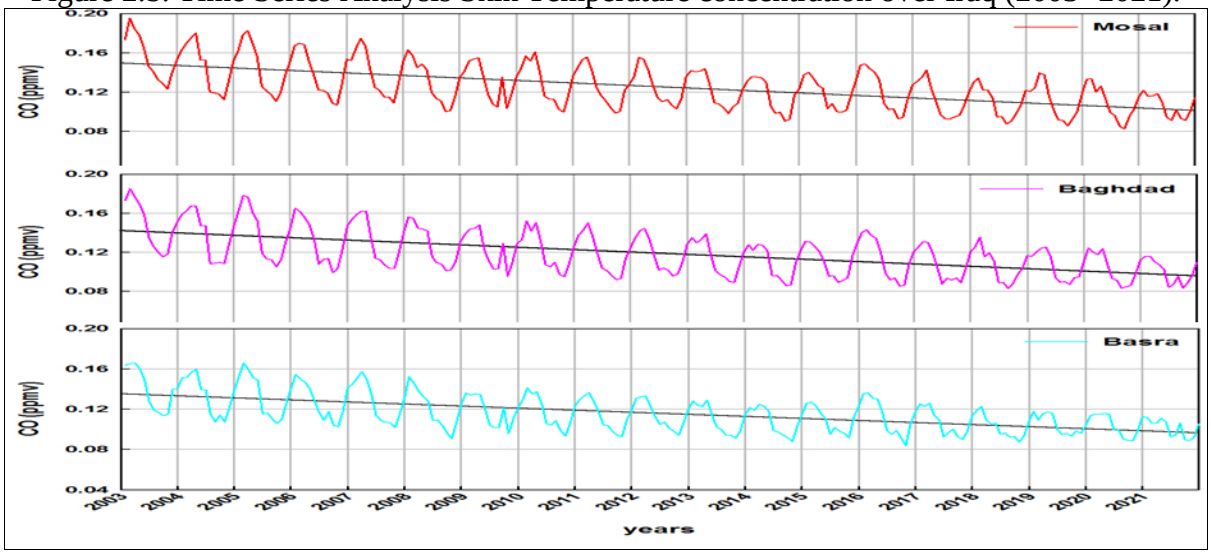

Figure 2.c. Time Series Analysis CO concentration over Iraq (2003 -2021).

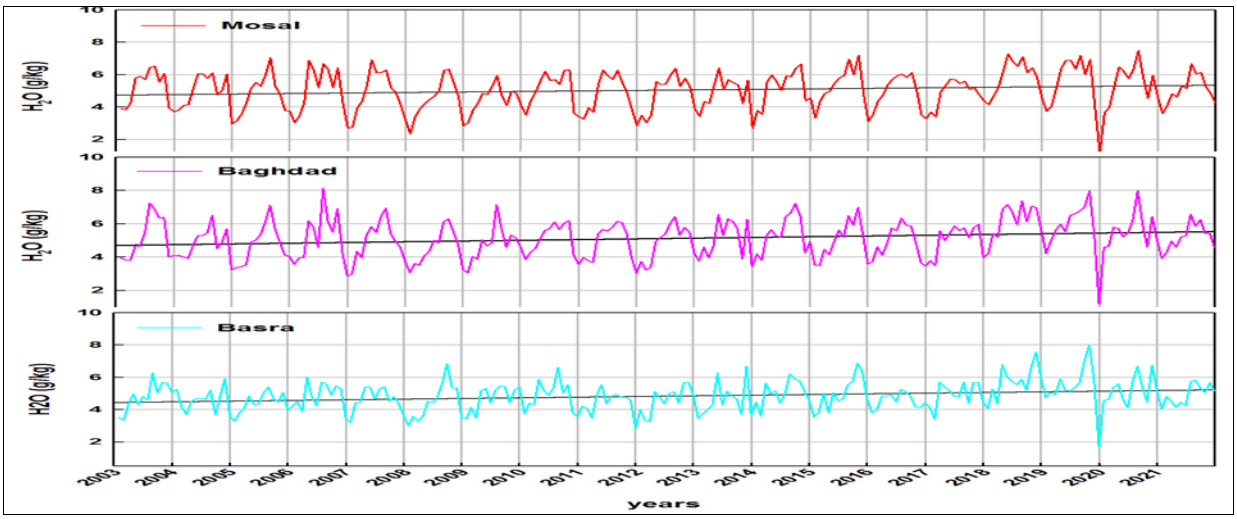

Figure 2.d. Time Series Analysis H2O concentration over Iraq (2003 -2021).

Maps of Spatial Distribution: To assess the spatial distribution of ozone, Skin Temp., CO and H_2Ovapor over Iraq, maps of the parameters were generated using the Kriging interpolation technique for monthly mean surface database observed for the study period for 19 years from2003- 2021(Winter, summer, spring and fall). The data were obtained from the AIRX3STM, 1º×1º spatial resolution ascending data in the lower troposphere. The mean seasonal data of retrieved ozone mixing ratio (O_3-VMR) was employed to map O_3 for a period of 19 years (2003-2021). As depicted in Figures 3, the ozone mixing ratio is lower during the winter season compared to the other seasons. In December, the lowest O_3 value over Iraq was recorded in the northern part of the country at 0.032 ppmv, as indicated in Figure 3. Conversely, during the spring season (April-May), the mean value of O3 was (0.048 ± 0.001) ppmv, marking the highest Value during the entire period. In the northern and northwestern regions of Iraq (above latitudes 34°N), the O_3 concentrations during April and May were approximately between 0.051 to 0.052 ppmv, whereas in the rest of Iraq, the levels ranged from 0.048 to 0.046 ppmv in the rest of the IRAQ areas.

Table 2. The Mann-Kendall statistical trend analysis was employed to estimate trends in O_3, Skin Temperature, CO and H_2O-vapor for the period between 2003 and 2021. The significance of change was determined at a 0.001 level of confidence**.**

Station O3 Month	**Mosel**		**Baghdad**		**Basra**	
	Z	**Q**	**Z**	**Q**	**Z**	**Q**
January	2.80	3.81E-04	2.56	5.74E-04	2.38	4.64E-04
February	2.31	2.36E-04	2.94	3.13E-04	3.01	4.36E-04
March	2.45	2.66E-04	2.38	2.84E-04	2.73	3.52E-04
April	1.82	3.37E-04	2.52	3.32E-04	2.73	3.75E-04
May	0.56	2.16E-02	2.31	4.14E-04	2.73	4.23E-04
June	2.24	3.41E-04	1.47	1.75E-04	2.52	3.00E-04
July	3.01	3.46E-04	3.08	3.89E-04	3.64	2.93E-04
August	3.57	4.61E-04	4.17	3.62E-04	4.52	2.96E-04
September	2.59	4.04E-04	2.31	5.02E-04	3.43	5.61E-04
October	3.85	2.37E-04	3.15	2.66E-04	2.59	1.64E-04
November	1.89	2.81E-04	1.96	3.52E-04	2.17	1.63E-04
December	1.68	2.24E-04	2.10	2.91E-04	1.54	2.53E-04

Table 3. The Mann-Kendall statistical trend analysis was employed to estimate trends in CO for the period between 2003 and 2021. The significance of change was determined at a 0.001 level of confidence.

Station CO Month	**Mosul**		**Baghdad**		**Basra**	
	Z	**Q**	**Z**	**Q**	**Z**	**Q**
January	-4.27	-2.49E-03	-2.54	-3.12E-03	-2.87	-2.64E-03

February	-5.25	-3.20E-03	-4.83	-3.19E-03	-4.87	-2.83E-03
March	-4.69	-3.44E-03	-4.97	-3.30E-03	-4.90	-2.91E-03
April	-4.76	-3.12E-03	-4.76	-2.83E-03	-4.69	-2.71E-03
May	-4.55	-2.59E-03	-4.62	-2.62E-03	-4.41	-1.87E-03
June	-5.32	-2.29E-03	-5.11	-2.28E-03	-4.62	-1.66E-03
July	-4.83	-1.97E-03	-5.18	-1.70E-03	-4.69	-1.27E-03
August	-4.76	-2.10E-03	-4.34	-1.82E-03	-3.36	-1.09E-03
September	-4.27	-1.90E-03	-4.55	-1.44E-03	-4.20	-1.11E-03
October	-4.13	-1.25E-03	-3.99	-1.40E-03	-3.71	-1.19E-03
November	-4.69	-1.94E-03	-4.62	-1.76E-03	-4.48	-1.75E-03
December	-4.69	-2.21E-03	-4.90	-2.14E-03	-4.69	-1.94E-03

Table 4. The Mann-Kendall statistical trend analysis was employed to estimate trends in Skin Temperature for the period between 2003 and 2021. The significance of change was determined at a 0.001 level of confidence.

Station SKIN T Month	**Mosul**		**Baghdad**		**Basra**	
	Z	**Q**	**Z**	**Q**	**Z**	**Q**
January	-1.75	-1.43E-01	1.30	1.53E-01	0.18	7.22E-02
February	0.77	7.29E-02	0.00	4.97E-03	0.70	5.73E-02
March	-1.26	-1.48E-01	-1.05	-1.07E-01	-0.21	-7.82E-03
April	0.67	7.29E-02	1.30	1.09E-01	0.95	4.57E-02
May	0.70	5.27E-02	2.31	1.86E-01	2.31	2.27E-01
June	2.17	1.97E-01	3.26	3.93E-01	3.22	3.90E-01
July	2.31	1.53E-01	3.82	3.99E-01	2.66	2.70E-01
August	1.89	7.50E-02	3.85	3.28E-01	2.45	1.80E-01
September	1.89	1.65E-01	3.57	3.63E-01	2.73	2.94E-01
October	-1.12	-7.88E-02	2.35	1.34E-01	0.67	5.47E-02
November	0.84	1.38E-01	1.68	1.69E-01	0.00	2.34E-03
December	-1.19	-1.20E-01	0.28	3.07E-02	0.14	2.00E-02

Table 5. The Mann-Kendall statistical trend analysis was employed to estimate trends in H_2O-vapor for the period between 2003 and 2021. The significance of change was determined at a 0.001 level of confidence.

Station H_2O Month	Mosel		Baghdad		Basra	
	Z	Q	Z	Q	Z	Q
January	1.61	3.56E-02	1.72	3.04E-02	1.46	3.82E-02
February	1.19	2.12E-02	1.54	4.85E-02	1.12	3.96E-02
March	2.45	6.26E-02	3.15	9.85E-02	2.17	6.95E-02
April	0.91	2.53E-02	0.98	3.12E-02	0.56	2.16E-02
May	0.56	2.13E-02	0.84	3.20E-02	1.05	3.12E-02
June	0.70	2.21E-02	2.77	6.54E-02	1.72	3.34E-02
July	0.70	1.58E-02	-0.07	-9.06E-03	2.24	3.82E-02
August	0.49	2.52E-02	-0.07	-2.13E-03	1.19	2.42E-02
September	1.23	3.73E-02	0.88	2.48E-02	0.67	2.02E-02
October	0.70	2.38E-02	0.84	3.93E-02	0.91	3.87E-02
November	1.12	4.92E-02	2.03	9.31E-02	1.47	5.35E-02
December	1.40	5.44E-02	1.19	5.00E-02	1.26	6.13E-02

During the summer months, the ozone level peaked with a mean value of (0.046±0.002) ppmv. However, as the fall season approached, specifically from September to November, the ozone mixing ratio began to decline gradually. Eventually, in November, it reached its lowest point at (0.035 ppmv) across most of IRAQ. The ozone mixing ratio across IRAQ exhibits latitudinal gradients throughout the year, with higher values observed in the northern regions during the spring and summer seasons. Conversely, the southern regions experience lower values during the fall and winter seasons. These variations can be attributed to the diverse weather conditions and topography, which play a significant role in influencing tropospheric ozone levels over IRAQ. The examination of Skin Temperature patterns across the seasons reveals that the Winter season consistently exhibits the lowest values throughout the study area and its surroundings. In this season, the temperature reaches a minimum of approximately (275 k). However, in the southern region, there is a notable increase in temperatures during February, with relatively high values peaking at (296 k). Figure 4 illustrates the progressive intensification of Skin Temperature levels during the spring season. Notably, the southern part of IRAQ experienced the highest recorded value, reaching (322 k). The most notable surge in Skin Temperature occurred predominantly during May, especially in the south and southwest regions, where it peaked at (328 k). However, the highest mean Skin Temperature values were observed during the summer season, particularly in July and August, reaching (332 k) across most regions of IRAQ. During the fall season, there

is a decline in the mean values of Skin Temperature. In November, this decline reaches its lowest point, with mean values dropping to (286 k) across most regions of IRAQ.

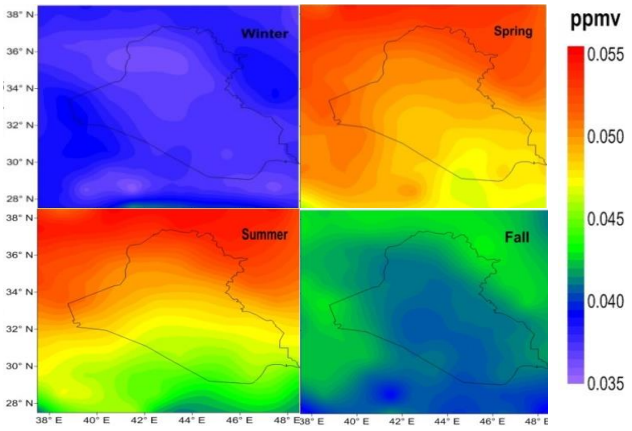

Figure 3. AIRS average seasonal coverage from the retrieved O_3, over Iraq for winter, spring, summer and fall seasons during 2003-2021.

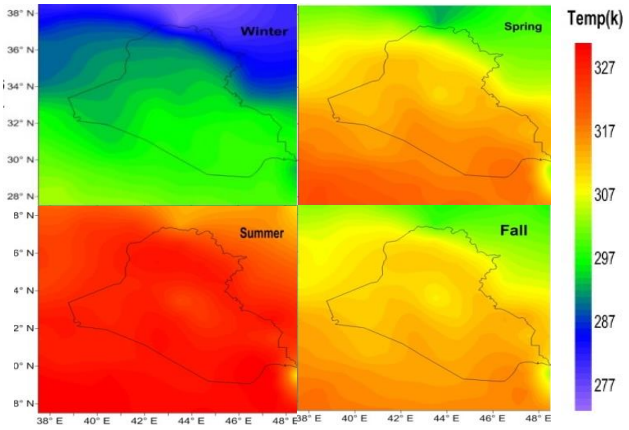

Figure 4. AIRS average seasonal coverage from the retrieved Skin Temp. Over Iraq for winter, spring, summer, and fall seasons during 2003-2021.

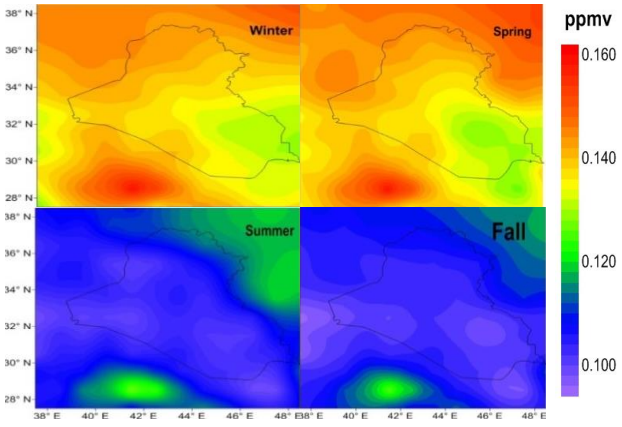

Figure 5. AIRS average seasonal coverage from the retrieved CO, over Iraq for winter, spring, summer and fall seasons during 2003-2021.

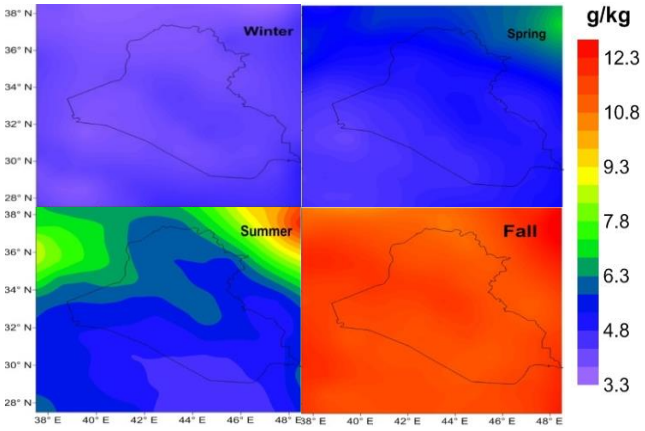

Figure 6. AIRS average seasonal coverage from the retrieved H_2Ovapor, over Iraq for winter, spring, summer and fall seasons during 2003-2021.

Figure 5 illustrates the AIRS coverage of retrieved CO VMR (Volume Mixing Ratio) during the winter and spring seasons. The mean CO value during this period is recorded as (0.149 ± 0.001) ppmv, making it the highest value observed throughout the entire yearly cycle for the study area. Notably, the northern region of IRAQ exhibits the highest CO values compared to other regions, reaching up to (0.162 ppmv) during the spring season. During the fall season, the mean value of CO is measured at (0.105 ± 0.01) ppmv, marking the lowest level observed throughout the entire period. In the summer seasons, the mean CO value slightly increases to (0.106 ± 0.01) ppmv. The highest CO values occur during the winter and spring seasons, particularly in the northern area, owing to the combined influence of meteorological conditions and the geographic nature of these regions. During these seasons, CO concentrations are significantly affected by plumes originating from Turkey and Syria, carried by the northwesterly winter Shamal wind. As the summer and fall seasons progress, CO emissions gradually decrease due to various influencing factors. One of these factors is the negative correlation between CO and surface temperature.

Additionally, the direct influence of hot and dusty southern and southeasterly winds with extensive vertical mixing and large-scale dynamics over wide areas contributes to the reduction of CO concentrations during this period. Moreover, the presence of CO precursors, especially the reaction between CO and OH radicals, further contributes to the decrease in CO levels during the summer and fall seasons. Water vapor (H_2Ovapor): The mean monthly data of water vapor mass mixing ratio (H_2Ovapor_MMR) were employed to create a map of H_2Ovapor distribution in the lower troposphere for a span of 19 years (2003-2021). According to Figure 6, the winter season consistently exhibits the lowest values of H_2Ovapor throughout the entire study area and its surrounding regions. The H_2Ovapor content remains relatively constant at approximately (3.32 ± 0.25) g/kg. During the winter season, the low temperatures cause significant condensation of water vapor, leading to its reduction to the lowest values observed throughout the year. In the spring season, minimum values are observed in the western and southern regions, primarily influenced by specific weather conditions that limit the formation of H_2Ovapor. However, there is a slight increase in H_2Ovapor over the north and northeast regions in April, and in May, this increase extends to the northern and central parts of IRAQ. As depicted in Figure 6b, the summer seasons (June - August) exhibit the highest mean values of H_2Ovapor, reaching (6.58 g/kg). These elevated values are observed across almost all regions of IRAQ, except for the south and southwest regions. Particularly in August, the H_2Ovapor content ranges between (5.52 to 6.69) g/kg, showcasing its peak during this period. Conversely, the lowest value of H_2Ovapor (4.88 g/kg) is observed in June, primarily in the south, southwest, and southeast regions. During the fall season, there is a noticeable increase in H_2Ovapor, reaching (6.43 g/kg) in September and (5.52 g/kg) in October across the same area, as illustrated in Figure 6b. However, in November, H2Ovapor starts to decrease, reaching its minimum value of approximately (4.22 g/kg) over the entirety of IRAQ, except for the southern regions bordering Kuwait. One of the primary reasons for the higher H2Ovapor levels during this period can be attributed to the strong evapotranspiration source at the surface, coinciding with an increase in temperature.

Conclusions

Over the 19-year study period, monthly averages were measured for O_3, Skin Temp, CO and H_2O-vapor surface mixing ratios in the study area, with mean and standard deviation values of (0.04 ± 0.002) ppmv for O_3, (310.85 ± 5.11) k for Skin Temp, (0.123 ± 0.005) ppmv for CO, and (4.99 ± 0.47) g/kg for H_2O-vapor. The annual means of these parameters were also calculated. The monthly distribution of these parameters exhibits notable temporal fluctuations in their values, with the highest values observed during the summer and the lowest values during the winter for both Skin Temperature and H2O-vapor. The maximum values for O_3 were recorded in spring, while the minimum values were observed in winter. CO reached its peak values during the winter, while the minimum values were observed in the fall. Spatially, all parameters except for AST and Skin Temperature had higher values in the northern regions and lower values in the southern regions of Iraq. Trend analysis revealed an increasing trend in Skin Temperature and H_2O-vapor, while O_3 remained almost constant with no significant trend observed. CO showed a significant negative trend for all stations.

References

Abbas, N., S. A. Wasimia & N. J. E. Al-Ansari (2016) Assessment of climate change impacts on water resources of Al-Adhaim, Iraq using SWAT model. 8**,** 716-732.

Abbas, N. M. & J. M. Rajab (2022) Sulfur Dioxide (SO_2) anthropogenic emissions distributions over Iraq (2000-2009) using MERRA-2 data. *Al-Mustansiriyah Journal of Science,* 33**,** 27-33.

Abdulfattah, I. S., J. M. Rajab, A. M. Al-Salihi, A. Suliman & H. S. Lim (2020) Observed vertical distribution of tropospheric carbon monoxide during 2012 over Iraq. *Przegląd Naukowy Inżynieria i Kształtowanie Środowiska,* 29.

Al-Bayati, R. M. & A. M. Al-Salihi. 2019. Monitoring carbon dioxide from (AIRS) over Iraq during 2003-2016. In *AIP Conference Proceedings*. AIP Publishing.

Al-Faraj, F. A., D. Tigkas & M. J. E. P. Scholz (2016) Irrigation efficiency improvement for sustainable agriculture in changing climate: a transboundary watershed between Iraq and Iran. 3**,** 603-616.

Ali. j. M., Samir k. M., and Jasim H. K. (2021) Dynamical Study for Selective Extreme Events over Iraq and Their Relations with General Circulations, Al-Mustansiriyah Journal of Science, Vol. 32, Issue 2.

Al-Salihi, A. M., J. M. Rajab & Z. Q. Salih. 2019. Satellite monitoring for Outgoing Longwave Radiation and Water Vapor during 2003-2016 in Iraq. In *Journal of Physics: Conference Series*, 012009. IOP Publishing.

Al Khudhairy, A. A. J. A.-M. J. o. S. (2018) Spatio-temporal analysis of Maximum temperature over Iraq. 29**,** 1-8.

Aumann, H. H., M. T. Chahine, C. Gautier, M. D. Goldberg, E. Kalnay, L. M. McMillin, H. Revercomb, P. W. Rosenkranz, W. L. Smith, D. H. J. I. T. o. G. Staelin & R. Sensing (2003) AIRS/AMSU/HSB on the Aqua mission: Design, science objectives, data products, and processing systems. 41**,** 253-264.

Azooz, A., S. J. J. o. E. P. Talal & S. Development (2015) Evidence of climate change in Iraq. 1**,** 66-73.

Borhani, F., M. Shafiepour Motlagh, A. Stohl, Y. Rashidi & A. H. Ehsani (2021) Tropospheric Ozone in Tehran, Iran, during the last 20 years. *Environmental Geochemistry and Health***,** 1-23.

Chen, B., Y. Wang, J. Huang, L. Zhao, R. Chen, Z. Song & J. Hu (2023) Estimation of near-surface ozone concentration and analysis of main weather situation in China based on machine learning model and Himawari-8 TOAR data. *Science of The Total Environment,* 864**,** 160928.

David, L. M. & P. R. J. J. o. G. R. A. Nair (2011) Diurnal and seasonal variability of surface ozone and NOx at a tropical coastal site: Association with mesoscale and synoptic meteorological conditions. 116.

Fiore, A. M., V. Naik, D. V. Spracklen, A. Steiner, N. Unger, M. Prather, D. Bergmann, P. J. Cameron-Smith, I. Cionni & W. J. Collins (2012) Global air quality and climate. *Chemical Society Reviews,* 41**,** 6663-6683.

Firas S. Basheer, "Trend Analysis of Annual Surface Air Temperature for Some Stations over Iraq," Al-Mustansiriyah Journal of Science, vol. 33, pp. 77-82, 2022.

Gilbert, R. O. 1987. *Statistical methods for environmental pollution monitoring*. John Wiley & Sons.

Gulev S., P. Thorne , J. Ahn, F. Dentener, C. Domingues, S. Gerland, D. Gong, D. Kaufman, H. Nnamchi, J. Quaas, J. Rivera, S. Sathyendranath, S. Smith, B. Trewin, K. V. Schuckmann, and R. Vose (2021) Changing State of the Climate System, Cambridge

University Press, Cambridge, United Kingdom and New York, NY, USA, p 1363-1512. https:// doi. org/ 10. 1017/ 97810 09157 896. 004.

Jin, M., R. E. Dickinson & D. J. J. o. c. Zhang (2005) The footprint of urban areas on global climate as characterized by MODIS. 18**,** 1551-1565.

Jin, M. & R. E. J. E. r. l. Dickinson (2010) Land surface skin temperature climatology: Benefitting from the strengths of satellite observations. 5**,** 044004.

Jin, M. & R. E. J. G. R. L. Dickinson (2002) New observational evidence for global warming from satellite. 29**,** 39-1-39-4.

Kadhum, J. H., M. F. Al-Zuhairi, A. A. J. M. E. S. Hashim & Environment (2022) Synoptic and dynamic analysis of few extreme rainfall events in Iraq. 8**,** 4939-4952.

Kajii, Y., K. Someno, H. Tanimoto, J. Hirokawa, H. Akimoto, T. Katsuno & J. J. G. R. L. Kawara (1998) Evidence for the seasonal variation of photochemical activity of tropospheric ozone: Continuous observation of ozone and CO at Happo, Japan. 25**,** 3505-3508.

Kirschke, S., P. Bousquet, P. Ciais, M. Saunois, J. G. Canadell, E. J. Dlugokencky, P. Bergamaschi, D. Bergmann, D. R. Blake & L. Bruhwiler (2013) Three decades of global methane sources and sinks. *Nature geoscience,* 6**,** 813-823.

Lim H.S., J. M. Rajab, A. M. Al-Salihi, S. Zainab, and M. MatJafri (2022) A statistical model to predict and analyze air surface temperature based on remotely sensed observations, Environ Sci Pollut Res 29, 9755–9765.

Lim H.S., M. MatJafri, A. Khiruldden, A. N. Alias, J. M. Rajab, and S. N. Mohd (2008) Algorithm for TSS mapping using satellite data for Penang Island Malaysia, Fifth International Conference on Computer Graphics Imaging and Visualization 978-0-7695-3359-9/08 IEEE DOI 10.1109/CGIV.2008.18 376-379.

Liu, J., S. A. Strode, Q. Liang, L. D. Oman, P. R. Colarco, E. L. Fleming, M. E. Manyin, A. R. Douglass, J. R. Ziemke & L. N. Lamsal (2022) Change in Tropospheric Ozone in the Recent Decades and Its Contribution to Global Total Ozone. *Journal of Geophysical Research: Atmospheres,* 127**,** e2022JD037170.

Lu, X., D. J. Jacob, Y. Zhang, J. D. Maasakkers, M. P. Sulprizio, L. Shen, Z. Qu, T. R. Scarpelli, H. Nesser & R. M. Yantosca (2021) Global methane budget and trend, 2010–2017: complementarity of inverse analyses using in situ (GLOBALVIEWplus CH< sub> 4</sub> ObsPack) and satellite (GOSAT) observations. *Atmospheric Chemistry and Physics,* 21**,** 4637-4657.

Mojid M. A., Parvez M. F., M. Mohammed, and H. Geoff (2019) Water Table Trend—A Sustainability Status of Groundwater Development in North-West Bangladesh, Water 11, no. 6: 1182.

Panos H., T. Anna, Z. George, and L. Jos (2023) Urbanisation and Geographical Signatures in Observed Air Temperature Station Trends Over the Mediterranean and the Middle East–North Africa, Earth Syst Environ, https://doi.org/10.1007/s41748-023-00348-y.

Park, Y.C., Y.J. Jo, and J.Y. Lee (2011) Trends of groundwater data from the Korean National Groundwater Monitoring Stations: indication of any change? Geosciences Jour., v.15(1), pp.105-114.

Rahman, A., M. Kamruzzama, C.S. Jahan, and Q.H. Mazumder (2016) Long-term trend analysis of water table using 'MAKESENS' model and sustainability of groundwater resources in drought prone Barind area, NW Bangladesh. J Geol Soc India 87, 179–193.

Rajab, J. M., M. Jafri, H. Lim & K. Abdullah (2011a) Monthly distribution map of carbon monoxide (CO) from AIRS over Peninsular Malaysia, Sabah and Sarawak for the year 2003. *Pertanika Journal of Science and Technology,* 19**,** 89-96.

Rajab, J. M., M. MatJafri, H. Lim, K. Abdullah & F. M. Hassan (2011b) Carbon monoxide mixing ratio variations over Peninsular Malaysia from AIRS observation: 2003–2009. In *Proceeding of the 2011 IEEE International Conference on Space Science and Communication (IconSpace)*, 142-146. IEEE.

Rajab, J. M., M. MatJafri, F. Tan, H. Lim & K. Abdullah (2011c) Analysis of Ozone column burden in Peninsular Malaysia retrieved from Atmosphere Infrared Sounder (AIRS) data: 2003–2009. In *2011 IEEE International Conference on Imaging Systems and Techniques*, 29-33. IEEE.

Rajab, J. M., H. Lim & M. MatJafri (2013) Monthly distribution of diurnal total column ozone based on the 2011 satellite data in Peninsular Malaysia. The Egyptian Journal of Remote Sensing and Space Science, 16, 103-109.

Rajab, J. M., A. S. Hassan, J. H. Kadhum, A. M. Al-Salihi & H. San Lim (2020) Analysis of tropospheric NO_2 over Iraq using OMI satellite measurements. Scientific Review Engineering and Environmental Sciences, 2020, 3-16.

Rypdal, K., T. Berntsen, J. S. Fuglestvedt, K. Aunan, A. Torvanger, F. Stordal, J. M. Pacyna, L. P. J. E. S. Nygaard & Policy (2005) Tropospheric ozone and aerosols in climate agreements: scientific and political challenges. 8**,** 29-43.

Safieddine, S., A. Boynard, N. Hao, F. Huang, L. Wang, D. Ji, B. Barret, S. D. Ghude, P.-F. Coheur & D. Hurtmans (2016) Tropospheric ozone variability during the East Asian summer monsoon as observed by satellite (IASI), aircraft (MOZAIC) and ground stations. *Atmospheric Chemistry and Physics,* 16**,** 10489-10500.

Salih, Z., A. M. Al-Salihi & J. M. Rajab (2018) Assessment of Troposphere Carbon Monoxide variability and trend in Iraq using Atmospheric Infrared Sounder during 2003-2016. *Journal of Environmental Science and Technology,* 11**,** 39-48.

Salman, S. A., M. M. Hamed, S. Shahid, K. Ahmed, A. Sharafati, M. Asaduzzaman, G. F. Ziarh, T. Ismail, E. S. Chung & X. J. J. I. J. o. C. Wang (2022) Projecting spatiotemporal changes of precipitation and temperature in Iraq for different shared socioeconomic pathways with selected Coupled Model Intercomparison Project Phase 6. 42**,** 9032-9050.

Salmi, T. 2002. *Detecting trends of annual values of atmospheric pollutants by the Mann-Kendall test and Sen's slope estimates-the Excel template application MAKESENS*. Ilmatieteen laitos.

Stavert, A. R., M. Saunois, J. G. Canadell, B. Poulter, R. B. Jackson, P. Regnier, R. Lauerwald, P. A. Raymond, G. H. Allen & P. K. Patra (2022) Regional trends and drivers of the global methane budget. *Global change biology,* 28**,** 182-200.

Stock, Z., M. Russo, T. M. Butler, A. Archibald, M. G. Lawrence, P. Telford, N. Abraham & J. Pyle (2013) Modelling the impact of megacities on local, regional and global tropospheric ozone and the deposition of nitrogen species. *Atmospheric Chemistry and Physics,* 13**,** 12215-12231.

Strahan, S. E. & A. R. Douglass (2018) Decline in Antarctic ozone depletion and lower stratospheric chlorine determined from Aura Microwave Limb Sounder observations. *Geophysical Research Letters,* 45**,** 382-390.

Susskind, J., G. Schmidt, J. Lee & L. J. E. R. L. Iredell (2019) Recent global warming as confirmed by AIRS. 14**,** 044030.

Vollmer, M. K., J. Mühle, S. Henne, D. Young, M. Rigby, B. Mitrevski, S. Park, C. R. Lunder, T. S. Rhee & C. M. Harth (2021) Unexpected nascent atmospheric emissions of three ozone-depleting hydrochlorofluorocarbons. *Proceedings of the National Academy of Sciences,* 118**,** e2010914118.